Anisotropic intrinsic anomalous Hall effect in ordered 3*d*Pt alloys

Hongbin Zhang,* Stefan Blügel, and Yuriy Mokrousov
Peter Grünberg Institut and Institute for Advanced Simulation, Forschungszentrum Jülich and JARA, D-52425 Jülich, Germany
(Received 25 March 2011; published 1 July 2011)

By performing first-principles calculations, we investigate the intrinsic anomalous Hall conductivity (AHC) and its anisotropy in ordered $L1_0$ FePt, CoPt, and NiPt ferromagnets and their intermediate alloys. We demonstrate that the AHC in this family of compounds depends strongly on the direction of the magnetization **M** in the crystal. We predict that such pronounced orientational dependence in combination with the general decreasing trend of the AHC when going from FePt to NiPt leads to a sign change of the AHC upon rotating the magnetization direction in the crystal of CoPt alloy. We also suggest that, for a range of concentration x in $Co_xNi_{1-x}Pt$ and $Fe_xCo_{1-x}Pt$ alloys, it is possible to achieve a complete quenching of the anomalous Hall current for a certain direction of the magnetization in the crystal. By analyzing the spin-resolved AHC in 3*d*Pt alloys, we endeavor to relate the overall trend of the AHC in these compounds to the changes in their densities of *d* states around the Fermi energy upon varying the atomic number. Moreover, we show the generality of the phenomenon of anisotropic anomalous Hall effect by demonstrating its occurrence within the three-band tight-binding model.

DOI: 10.1103/PhysRevB.84.024401 PACS number(s): 75.47.−m, 71.20.Be, 72.15.Gd

I. INTRODUCTION

Despite its long history, the anomalous Hall effect (AHE) in ferromagnets, discovered in 1881,[1] is still not fully understood from the theoretical point of view.[2] Nevertheless, due to possible vast applications in spintronic devices, the AHE, and its counterpart in nonmagnetic materials, the spin Hall effect (SHE),[3] have drawn quite intensive attention in recent years. The underlying topological nature of the intrinsic AHE and SHE, relating these phenomena to some fundamental physical effects, makes them even more relevant and interesting. Spin-orbit coupling (SOC) plays a crucial role in both AHE and SHE, as proposed in the first microscopic theory of the AHE by Karplus and Luttinger.[4] It can be demonstrated that SOC in perfect crystals gives rise to a transverse anomalous velocity of electrons propagating along the direction of the external electric field, thus leading to the anomalous Hall current. This mechanism is nowadays referred to as the intrinsic contribution.

The intrinsic AHC considered in this paper can be obtained via the linear response Kubo formula for the off-diagonal components of the conductivity tensor σ:

$$\begin{aligned}\sigma_{ij} &= -e^2\hbar\int_{\mathrm{BZ}}\frac{d^3k}{8\pi^3}\,\Omega_{ij}(\mathbf{k}),\\ \Omega_{ij}(\mathbf{k}) &= -2\mathrm{Im}\sum_{n,m}^{o,e}\frac{\langle\psi_{n\mathbf{k}}\mid v_i\mid\psi_{m\mathbf{k}}\rangle\langle\psi_{m\mathbf{k}}\mid v_j\mid\psi_{n\mathbf{k}}\rangle}{(\varepsilon_{n\mathbf{k}}-\varepsilon_{m\mathbf{k}})^2},\end{aligned}\tag{1}$$

which relates the conductivity tensor to the Brillouin zone (BZ) integral of the **k**-dependent Berry curvature tensor Ω. In the latter expression, $\psi_{n\mathbf{k}}$ and $\psi_{m\mathbf{k}}$ are, respectively, the occupied (o) and empty (e) one-electron spinor Bloch eigenstates of the crystal, $\varepsilon_{n\mathbf{k}}$ and $\varepsilon_{m\mathbf{k}}$ are their eigenenergies, and v_i and v_j are the Cartesian components of the velocity operator **v**. As a second-rank antisymmetric tensor, the AHC tensor can be also seen as the anomalous Hall conductivity vector $\boldsymbol{\sigma}$, the components of which are related to the components of the AHC as $\sigma_i = \frac{1}{2}\epsilon_{ijk}\sigma_{jk}$, where ϵ_{ijk} is the Levi-Civita tensor.

For materials with impurities or disorder, extrinsic contributions to the AHE also exist, which can be described within density-functional theory.[5,6] Nevertheless, the intrinsic contribution is often dominating in itinerant ferromagnets with moderate resistivity.[2] Since the intrinsic anomalous Hall conductivity (AHC) is determined by the electronic structure of a pristine crystal [Eq. (1)], which can be accurately calculated using modern first-principles methods, a comparison between experiments and first-principles calculations serves as the first necessary step to deeper understanding of the intrinsic AHE in real materials. Several investigations using the first-principles methods have been done, for instance, in $SrRuO_3$,[7,8] Fe,[9,10] Mn_5Ge_3,[11] $CuCr_2Se_{4-x}Br_x$,[12] Ni,[13] and Co.[13,14] For those materials, the calculated intrinsic AHC agrees well with the experimental values, except for the case of fcc Ni,[13] which might be due to its complicated electronic structure.[15]

One of the recently emerging topics in the field of the transverse magnetotransport phenomena is the anisotropic nature of the off-diagonal part of the conductivity tensor.[14,16,17] In the case of the AHE, the presence of the magnetization **M** in a ferromagnet leads to a strong dependence of the components of the conductivity tensor on the magnetization direction in the sample. Although experimentally, anisotropic AHE has been observed in many materials, e.g., bcc Fe,[18] fcc Ni,[19,20] hcp Gd,[21] as well as $FeCr_2S_4$,[22] $Yb_{14}MnSb_{11}$,[23] $Y_2Fe_{17-x}Co_x$,[24] and R_2Fe_{17} (R = Y, Tb, Gd),[25] only two studies of the anisotropy of the AHE from first principles have been performed so far. Roman *et al.*[14] considered the anisotropic AHE in uniaxial hcp Co, calculated the ratio of the AHCs for the out-of-plane and in-plane magnetization, σ_z and σ_x, respectively, and found it to be as large as four, which is close to the experimentally observed ratio.[19] Moreover, they performed a directional averaging of the anisotropic AHC and compared the obtained conductivity to the experimental value measured in polycrystalline hcp Co samples,[26] finding an excellent agreement.[14] In another work, Zhang and co-authors[17] considered the anisotropic AHE in uniaxial $L1_0$ FePt alloy. They also found a large anisotropy of the AHC in this compound, and were able to attribute it to the spin-nonconserving part of the spin-orbit interaction, prominent in this material with strong SOC.

In this paper, we undertake a detailed first-principles analysis of the anisotropic intrinsic AHE in the group of $L1_0$-ordered $3d$Pt ($3d$ = Fe, Co, Ni) alloys. These materials are currently under investigation with respect to possible spintronic applications due to their large uniaxial magnetic anisotropy energies and high Kerr rotation, making them possible candidates for ultrahigh density magnetic and magneto-optical recording media.[27] Recently, the AHE in FePt was used for injection of a spin-polarized current for consequent detection of direct and inverse spin Hall effect in Au.[28] In a combined experimental and theoretical study,[29] it was shown that the intrinsic contribution to the anomalous Hall signal dominates in samples of FePt with finite structural disorder. All this motivated our study of the anisotropy of the intrinsic AHE in uniaxial $3d$Pt alloys.

In general, we find very large anisotropy of the AHE in these compounds, which changes its magnitude and sign as a function of the band filling of the $3d$ transition metal. In particular, we observe that, for the $3d$Pt alloys with high concentration of Co atoms, the σ_z and σ_x conductivities differ in sign, which leads to the phenomenon of the *antiordinary* AHE, in which at a certain "magic" angle of the magnetization the Hall current **J** becomes parallel to **M**. Moreover, for $(Fe_{0.1}Co_{0.9})$Pt and $(Co_{0.85}Ni_{0.15})$Pt alloys, we predict the occurrence of the *colossal* anisotropy of the AHE, that is, an order of magnitude reduction in the value of σ_x as compared to σ_z, or vice versa. By analyzing the spin-resolved AHC in these alloys, we try to relate the general trend of decreasing AHC in these compounds when going from FePt to NiPt to the changes in their densities of states around the Fermi energy. Moreover, we demonstrate the occurrence of the anisotropic AHE within the uniaxial minimal three-band tight-binding model, which underlines the generality of this phenomenon and hints at its occurrence in a wide range of materials.

The structure of the paper is as follows. In Sec. II, we describe the method and details of our first-principles calculations. In Sec. III, we introduce a minimal three-band t_{2g} model, necessary to predict the appearance of the anisotropy of the AHE in a three-dimensional crystal, and investigate the AHC within this model as a function of the band filling. In Sec. IV, we present the results of our *ab initio* calculations of the AHE in the family of ordered FePt, CoPt, and NiPt alloys. We demonstrate that the AHE in these alloys is strongly anisotropic and displays a number of interesting phenomena in the region where it changes sign. We end the paper with conclusions.

II. COMPUTATIONAL DETAILS

We performed our density-functional theory (DFT) calculations of $L1_0$-ordered $3d$Pt ($3d$ = Fe, Co, Ni) alloys using the full-potential linearized augmented plane-wave (FLAPW) method as implemented in the Jülich DFT code FLEUR.[30] The generalized gradient approximation[31] (GGA) for the exchange-correlation potential was used. The self-consistent calculations with SOC were done in second variation with $k_{\max}$ of 4.0 a.u.$^{-1}$ and 16 000 k points in the full Brillouin zone. The muffin-tin radius of 2.45 a.u. was used for all atoms. Six local orbitals for the $4p$ states of Pt atoms were used to take care of the core charge of Pt correctly. In all our calculations, a tp_2 geometry with two atoms in the $L1_0$ phase was used for all alloys, with experimental lattice constants (Fig. 1).[32] For intermediate alloys, for instance, $(Fe_{0.5}Co_{0.5})$Pt, the virtual crystal approximation (VCA) was applied on the $3d$ atomic sites, where the composition-averaged core potential is used instead of that of pure $3d$ elements, together with the corresponding number of valence electrons and interpolated lattice constants from the neighboring compounds.

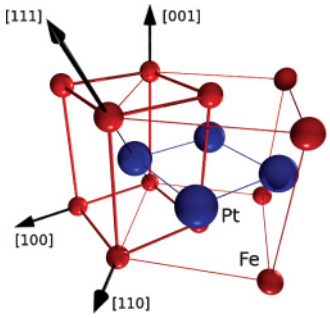

FIG. 1. (Color online) Crystal structure of $L1_0$ FePt alloy. Small (red) spheres stand for the Fe atoms, while large (blue) spheres mark the Pt ions. The primitive unit cell used in the calculations is enclosed with thicker lines. In the text, z stands for the [001] axis, while x stands for the [110] direction in the crystal.

In this paper, we applied the Wannier interpolation technique to calculate the AHC accurately. We followed the method introduced in Refs. 33 and 34 to construct the maximally localized Wannier functions (MLWFs) from the FLAPW wave functions, in which the unitary transformations are constructed to minimize the spread of the Wannier functions. Using the self-consistent charge density with SOC included, 36 MLWFs corresponding to s, p, and d orbitals of $3d$ and Pt atoms for both spins were generated on a $10 \times 10 \times 10$ k mesh, using the WANNIER90 code.[35] The AHC was then calculated by applying the Wannier interpolation scheme of Wang *et al.*[10] for evaluating the Berry curvature on a $208 \times 208 \times 208$ uniform k mesh. For k points at which the Berry curvature exceeded 30 Å^2, an adaptive refined k mesh of $5 \times 5 \times 5$ was used.

III. AHE ANISOTROPY: GENERALITIES

In terms of the AHC vector, the linear response expression for the anomalous Hall current **J** can be rewritten as

$$\mathbf{J}(\mathbf{M}) = \boldsymbol{\sigma}(\mathbf{M}) \times \mathbf{E}, \tag{2}$$

where **E** is the electric field. In a ferromagnet with uniform magnetization **M**, $\boldsymbol{\sigma}$ and **J** depend on the magnetization direction in the crystal. This magnetocrystalline anisotropy of the AHC manifests itself in the changes in the direction and magnitude of $\boldsymbol{\sigma}$ upon changing the direction of the magnetization away from a certain (easy) axis. In general, while **J** is always perpendicular to the electric field **E**, it is not necessarily orthogonal to **M**, as $\boldsymbol{\sigma}$ and **M** may not be parallel. In single crystals, $\boldsymbol{\sigma}$ and **M** are perfectly collinear only when **M** points along certain high-symmetry directions. For an arbitrary orientation of **M**, there is generally a misalignment between them, which is the signature of the anisotropic AHE. Another manifestation of the AHE anisotropy is the dependence of the

absolute value of $\mathbf{J}$ and $\boldsymbol{\sigma}$ on the direction of $\mathbf{M}$. While in cubic crystals the AHC anisotropy appears only at the third order with respect to the directional cosines of the magnetization, in uniaxial crystals the linear term can dominate,[14] leading to large AHE anisotropies, observed experimentally[19] and explained theoretically.[14]

The microscopic origin of the anisotropic AHE can be easily understood by inspecting Eq. (1). Consider a tetragonal crystal structure, as depicted for $L1_0$ FePt alloy in Fig. 1. Suppose that we start with the magnetization $\mathbf{M}$ pointing along the [001] axis (z axis in the following). In this case, the v_x and v_y components of the velocity operator have to be inserted at the place of v_i and v_j operators in Eq. (1) in order to obtain the σ_{xy} component of the conductivity tensor or, equivalently, the σ_z component of the conductivity vector, taking into account that, for such a high-symmetry direction of the magnetization, $\boldsymbol{\sigma}$ is aligned with $\mathbf{M}$ along the z axis. Rotating now $\mathbf{M}$ away from the [001] axis modifies (i) the wave functions $\psi_{n\mathbf{k}}$ and $\psi_{m\mathbf{k}}$, (ii) occupation of the states, and (iii) the eigenenergies of the states $\varepsilon_{n\mathbf{k}}$ and $\varepsilon_{m\mathbf{k}}$ due to the presence of the spin-orbit interaction. Thus, all components of the conductivity tensor have to be recalculated for a general direction of $\mathbf{M}$. In this paper, the magnetization is confined in the high-symmetry $(\bar{1}10)$ plane, and the resulting conductivity vector also lies in the same plane due to the antisymmetric nature of the anomalous Hall conductivity with respect to the inversion of the magnetization direction. For a general magnetization direction $\mathbf{M}$ in this plane, the AHC vector $\boldsymbol{\sigma}$ can be decomposed as follows:

$$\boldsymbol{\sigma} = \sigma_{\parallel}\hat{\mathbf{M}} + \sigma_{\perp}\mathbf{n}, \tag{3}$$

where $\hat{\mathbf{M}}$ and $\mathbf{n}$ are the unit vectors along the magnetization direction and orthogonal to it within the $(\bar{1}10)$ plane, respectively. The ratio of $\sigma_{\parallel}(\mathbf{M})$ and $\sigma_{\perp}(\mathbf{M})$ gives an estimate of how strongly the AHC vector deviates from the direction of $\mathbf{M}$. Upon further rotation, the magnetization hits the [110] direction in the crystal (x axis in the following), and the orthogonal component of the AHC $\sigma_{\perp}$ is zero, while $\boldsymbol{\sigma}$ is collinear with the magnetization again. In this case, v_y and v_z enter Eq. (1), and the magnitude of the AHC is given by σ_x.

IV. ANISOTROPIC AHE WITHIN THE t_{2g} MODEL

In this section, we demonstrate the appearance of anisotropic AHE within a simple tight-binding model, namely, three-band t_{2g} model for d_{yz}, d_{zx}, and d_{xy} spin-up orbitals on a cubic lattice. We consider only the hoppings up to the nearest neighbors t_1 and to the next-nearest neighbors t_2. The Hamiltonian of the model in k space reads as

$$H(\mathbf{k}) = H_0(\mathbf{k}) + H_{\mathrm{SO}}(\mathbf{M}), \tag{4}$$

where the Hamiltonian without SOC is given by

$$H_0(\mathbf{k}) = \begin{pmatrix} -2t_1(\cos k_y + \mathrm{A}\cos k_z) & 4t_2 \sin k_x \sin k_y & 4t_2 \sin k_x \sin k_z \\ 4t_2 \sin k_x \sin k_y & -2t_1(\cos k_x + \mathrm{A}\cos k_z) & 4t_2 \sin k_y \sin k_z \\ 4t_2 \sin k_x \sin k_z & 4t_2 \sin k_y \sin k_z & -2t_1(\cos k_x + \cos k_y) \end{pmatrix}, \tag{5}$$

in which we introduced an anisotropy parameter A. The role of this parameter is to make the system uniaxial, i.e., for $A \neq 1$, the nearest-neighbor hopping in the (x,y) plane is different from that along the z axis. In a real cubic crystal, introducing such a uniaxiality could correspond to, e.g., changing the interlayer distance along the z axis via application of stress.

The k-independent SOC part of the Hamiltonian depends on the magnetization direction $\mathbf{M}$ in the crystal. Within our model for $\mathbf{M}$ along the z axis, the $d_{yz}^{\uparrow}$ and $d_{zx}^{\uparrow}$ orbitals are coupled due to SOC, and the H_{SO} matrix reads as

$$H_{\mathrm{SO}}(\mathbf{M}\|z) = \xi \begin{pmatrix} 0 & i & 0 \\ -i & 0 & 0 \\ 0 & 0 & 0 \end{pmatrix}, \tag{6}$$

while for $\mathbf{M}$ along the x axis, $d_{zx}^{\uparrow}$ and $d_{xy}^{\uparrow}$ orbitals are coupled instead:

$$H_{\mathrm{SO}}(\mathbf{M}\|x) = \xi \begin{pmatrix} 0 & 0 & 0 \\ 0 & 0 & i \\ 0 & -i & 0 \end{pmatrix}. \tag{7}$$

The strength of the spin-orbit interaction is constant in both cases and is given by the parameter of the model ξ. The band structure of the model obtained by diagonalizing Hamiltonian (4) is plotted in Fig. 2 for $\mathbf{M}\|x$ and $A = 1$.

The AHC calculated according to Eq. (1) for the t_{2g} model is shown in Fig. 3 as a function of band filling for $\mathbf{M}\|z$ and $\mathbf{M}\|x$, both with $A = 1$ and 0.9. We assumed for our calculations a lattice constant of 1 Å, $t_2/t_1 = 0.1$, and $\xi/t_1 = 0.02$. Obviously, as expected from symmetry, the AHC does not depend on whether the magnetization points along the x or z axis when $A = 1$, while it displays a strong dependence on the electron occupation n or, equivalently, on the position of the Fermi level E_F^n, which corresponds to this occupation. Such sensitive dependence of intrinsic AHC on the details of the electronic structure, which stems from a very irregular behavior of the Berry curvature in the Brillouin zone, is rather well known.[2] From our calculations, it can be seen that when the Fermi energy is positioned in the vicinity of the band edges with high density of electronic states (DOS), which in our model corresponds to the case of nearly filled, half-filled, and completely filled bands, the E_F position has a strong effect on the AHC (Fig. 3). The reason behind such a sensitive dependence lies in the presence of flat degenerate bands around the Fermi energy, which provide wide regions in k space where the occupied and unoccupied states are separated by a small

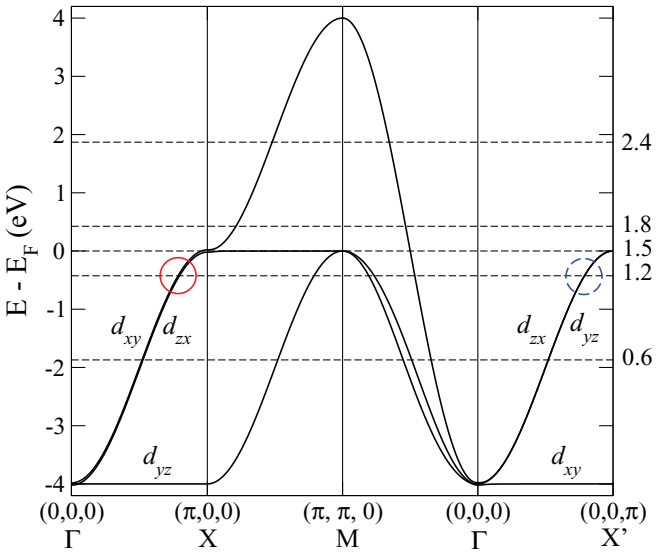

FIG. 2. (Color online) Electronic bands of the t_{2g} model for $\mathbf{M}\|x$, with $t_2/t_1 = 0.1$, $\xi/t_1 = 0.02$, $A = 1.0$, and the lattice constant of 1 Å. The dashed horizontal lines mark the position of the Fermi level for the electronic occupation given by the number on the right. Labels mark the orbital character of the bands.

energy. We speculate that such a situation can also be related to the anomaly of the density of states near the band edges and associated Lifshitz transitions.[36] We expect that, at such transitions, anomalies in the AHC would lead to, e.g., singular behavior of the anomalous thermopower.

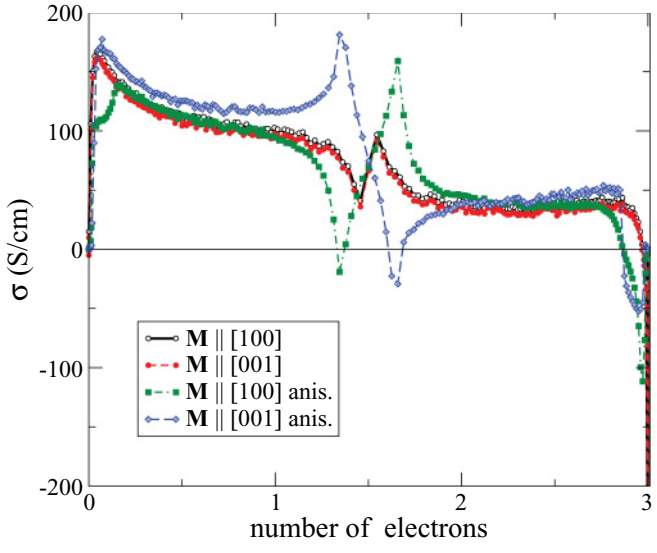

FIG. 3. (Color online) Anomalous Hall conductivity as a function of the band filling within the three-band t_{2g} model with the parameters given in the caption to Fig. 2. Open (filled) circles mark the case of $\mathbf{M}\|x(z)$ in the "isotropic" crystal with $A = 1$ in Eq. (4). Note that, in this case, the AHC curve for $\mathbf{M}\|z$ is shifted by 5 S/cm with respect to the AHC with $\mathbf{M}\|x$ in order to see the degeneracy between the two curves clearly. Filled squares (diamonds) stand for the AHC in the "anisotropic" crystal with $A = 0.9$ in Eq. (4) for $\mathbf{M}\|x(z)$.

In the case of the "uniaxial" t_{2g} model ($A = 0.9$), the electronic structure of the crystal with $\mathbf{M}\|x$ and $\mathbf{M}\|z$ is not the same anymore, and a strong anisotropy of the AHC can be seen in Fig. 3, leading even to a difference in sign, considered in detail in the following section. In analogy to the case of the "isotropic" crystal, the largest difference between the AHC for the two magnetization directions can be observed for $n \approx 0$, 1.5, and 3, although for exact half-occupation ($n = 1.5$), this difference vanishes.

In order to see the origin of the anisotropic AHC in the uniaxial t_{2g} crystal clearly, we refer to the band structure of the system, Fig. 2, for $\mathbf{M}\|x$ and $A = 1$. Let us consider the case of $n = 1.2$ and transitions between the occupied and unoccupied states in the energy region marked with a (red) solid-line circle along the ΓX path. For $\mathbf{M}\|x$, the SOC leads to the mixing of d_{xy} and d_{zx} orbitals, and the resulting small energy splitting between the two corresponding bands can be clearly seen. The nonvanishing matrix element of the SOC between the two latter orbitals leads to a finite contribution to the Berry curvature and the AHC associated with the electronic transitions across $E_F^{1,2}$. On the other hand, the d_{zx} and d_{yz} orbitals are not coupled by SOC for this magnetization direction (which can be also seen from an exact degeneracy of corresponding bands along $\Gamma X'$), and the contribution from the symmetry equivalent without SOC part of the band structure along $\Gamma X'$ to the Berry curvature, marked with a dashed-line (blue) circle, is exactly zero. The situation is reversed for $\mathbf{M}\|z$ in the isotropic crystal, and the contribution to the AHC from the states in the dashed-line (blue) circle is exactly the same as that from the corresponding region along the ΓX path for $\mathbf{M}\|x$, while the latter gives no contribution for $\mathbf{M}\|z$. Overall, when only the encircled regions and their symmetric "clones" are considered, the resulting AHC does not depend on the magnetization direction and there is no anisotropy of it. Introducing now anisotropy in the system by setting A to 0.9 in the t_{2g} model leads to the fact that the electronic structure along the ΓX and $\Gamma X'$ paths is not the same anymore and, thus, the contributions to the AHC from the solid-line (red) circle for $\mathbf{M}\|x$ and from the dashed-line (blue) circle for $\mathbf{M}\|x$ are different. In turn, this leads to the AHE anisotropy. This line of thinking is clearly valid also for explaining the anisotropy of the total AHC, which is obtained by a summation over all such encircled regions in energy and k space, contributing to the AHC.

V. ANISOTROPIC AHC IN 3*d*Pt ALLOYS

The results of our calculations for the intrinsic AHC in $L1_0$-ordered FePt, CoPt, and NiPt and their intermediate alloys are presented in Table I and in Fig. 4 for [001] (σ_z) and [110] (σ_x) directions of the magnetization $\mathbf{M}$ in the crystal. In general, the observed behavior of σ_z and σ_x as a function of the electron occupation of the 3*d* transition metal is similar: Starting from the FePt alloy with positive values of the AHC for both magnetization directions of around 600 S/cm, the sign of σ_z and σ_x changes in the vicinity of the CoPt alloy, and the AHC values are very large and negative for NiPt, reaching as much as -1200 S/cm. On average, we can see that the decrease of both conductivities with increasing electron occupation is rather linear. It is worth mentioning that such decreasing trend

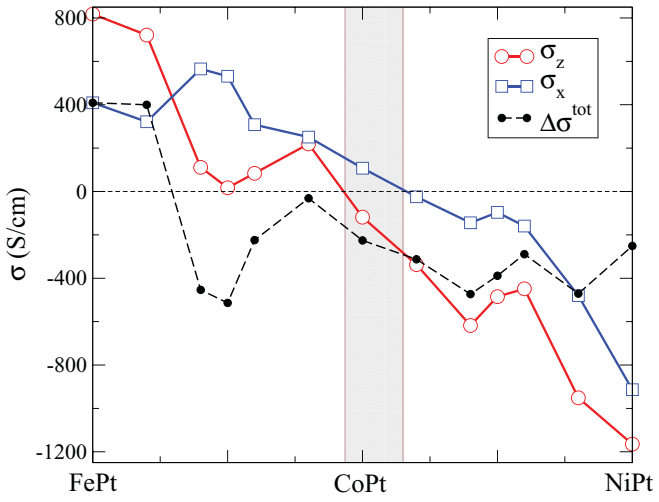

FIG. 4. (Color online) Anomalous Hall conductivity of 3*d*Pt alloys for **M** along [001] (σ_z, open circles) and [110] (σ_x, open squares), and anisotropy ($\Delta\sigma^{\rm tot} = \sigma_z - \sigma_x$, filled circles), with respect to the band filling.

of the AHC is somewhat reminiscent of the trend among the pure bcc Fe, hcp Co, and fcc Ni, for which the calculated intrinsic values of σ_z constitute approximately 750 S/cm,[9,10] 480 S/cm,[13,14] and −2200 S/cm,[13] respectively. We will come back to this point at the end of this section.

It is clear from Table I and Fig. 4 that, for almost all considered alloys, the anisotropy of the AHC reaches very large values. This is expected since, in uniaxial crystals, the AHC anisotropy appears already in the first order with respect to the directional cosines of the magnetization (see discussion in the previous section).[14] In FePt, the difference between σ_z and σ_x, $\Delta\sigma^{\rm tot}$ (filled circles in Fig. 4), is as large as σ_x itself and constitutes around 400 S/cm (cf. Table I).[17] In CoPt, on the other hand, the absolute value of $\Delta\sigma^{\rm tot}$ is twice larger than the absolute value of the AHC for any of the two magnetization directions. The AHC anisotropy reaches as much as −500 S/cm in the vicinity of FeCoPt and CoNiPt alloys, and, in general, the behavior of $\Delta\sigma^{\rm tot}$ is neither smooth nor monotonous, displays several mimina and maxima as a function of the electron occupation, and even changes its sign for $Fe_xCo_{1-x}Pt$ alloy with $x \approx 0.75$. On the other hand, the anisotropy of the AHE in 3*d*Pt alloys, when the magnetization is rotated in the (001) plane, is much smaller than the out-of-plane−in-plane anisotropy discussed previously, which can be easily understood taking into consideration the higher symmetry of the former situation. For example, the difference of the AHCs for **M** along [110] and [100] reaches at most 80 S/cm in NiPt alloy, being as small as −47 S/cm in CoPt and −16 S/cm in FePt.

TABLE I. Values of the AHC in $L1_0$ FePt, CoPt, and NiPt with the magnetization along [001] (σ_z) and [110] (σ_x). For each orientation, $\sigma^{\uparrow\uparrow}$ ($\sigma^{\uparrow\downarrow}$) is calculated by keeping only the first (second) term in the spin-orbit Hamiltonian [Eq. (8)], while both terms are kept when calculating $\sigma^{\rm tot}$. $\Delta\sigma^{\rm tot}$ is defined as $\sigma_z - \sigma_x$. $\Delta\sigma^{\uparrow\uparrow(\uparrow\downarrow)}$ is defined as the difference between the spin-conserving (spin-flip) parts of σ_z and σ_x. All values are in S/cm.

		$\sigma^{\rm tot}$	$\sigma^{\uparrow\uparrow}$	$\sigma^{\uparrow\downarrow}$	$\Delta\sigma^{\rm tot}$	$\Delta\sigma^{\uparrow\uparrow}$	$\Delta\sigma^{\uparrow\downarrow}$
FePt	σ_z	818	577	133	409	−9	317
	σ_x	409	585	−184			
CoPt	σ_z	−119	487	−513	−226	−7	−210
	σ_x	107	494	−303			
NiPt	σ_z	−1165	−1495	−550	−251	−1215	7
	σ_x	−914	−280	−557			

With the gray shaded area in Fig. 4, we highlight the region around the CoPt alloy, where both σ_z and σ_x change their sign. This sign change leads to the occurrence of two interesting phenomena with respect to the anisotropic AHE. The first one, which we name the *colossal anisotropy* of the AHE, according to our calculations, occurs for $Fe_xCo_{1-x}Pt$ alloy with $x \approx 0.1$ and for $Co_xNi_{1-x}Pt$ alloy with $x \approx 0.85$. For these two compounds, one of the conductivities, σ_z for $Fe_{0.1}Co_{0.9}Pt$ and σ_x for $Co_{0.85}Ni_{0.15}Pt$, turns to zero, which marks the complete disappearance of the intrinsic anomalous Hall current **J** for one of the magnetization directions in the crystal. We introduce the term colossal anisotropy in analogy to the situation that was predicted to occur in one-dimensional Pt wires for which, upon changing the magnetization direction **M**, the value of the magnetization |**M**| itself can be quenched completely.[37] In terms of the longitudinal transport within the setup of, e.g., an anisotropic magnetoresistance (AMR) experiment, the occurrence of the colossal anisotropy of the diagonal conductivity would result in a metal-insulator transition in the crystal; in the case of the colossal AHE anisotropy observed in 3*d*Pt alloys, all compounds remain metallic for all magnetization directions, however, and retain their complicated electronic structure around the Fermi energy.

For the $Co_{0.8}Ni_{0.2}Pt$ alloy in Fig. 5(a), we plot the dependence of the $\sigma_\parallel$ and $\sigma_\perp$ components of the AHC on the angle θ of the magnetization with the z axis when it is rotated away from the [001] direction within the $(\bar{1}10)$ plane towards the [110] direction. At $\theta = 0$, the $\sigma_\perp$ component is zero and the AHC vector with magnitude of 340 S/cm is antiparallel to the z axis, along which the magnetization is aligned [cf. Fig. 5(c)]. Upon increasing θ, we observe the increase in $\sigma_\parallel$ and decrease in $\sigma_\perp$, with both components becoming equal at the angle $\theta \approx 55^\circ$. At this angle, the magnitude of the AHC is reduced significantly to 210 S/cm, while its deviation from the z axis is only about 10°. Thus, in this range of θ, the rotation of the magnetization results mainly in quenching the magnitude of the anomalous Hall current, while its direction basically remains stuck to the [110] axis. Upon further rotation of the magnetization, both components of the AHC vector rapidly approach zero, the AHC vector quickly rotates toward the $-x$ axis, and when **M** hits the [110] direction, the AHC with a tiny magnitude of 25 S/cm is again antiparallel to the magnetization.

For CoPt alloy, the situation, depicted in Figs. 5(b)–5(e), is completely different. Similarly to the previously considered case, at $\theta = 0^\circ$ the AHC vector is antiparallel to **M**, and its magnitude constitutes 120 S/cm [Fig. 5(c)]. Upon increasing θ up to as much as 45°, the conductivity vector resides basically in the close vicinity of the $[00\bar{1}]$ axis, while its magnitude increases. For example, at $\theta = 45^\circ$, $\sigma_\parallel \approx \sigma_\perp$, and the value of

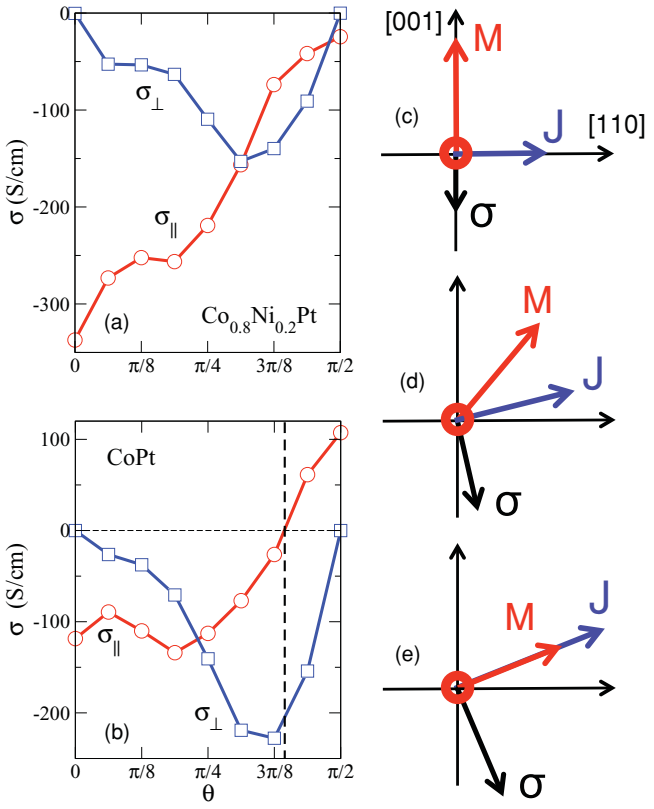

FIG. 5. (Color online) (a) Colossal anisotropy of the AHC in $Co_{0.8}Ni_{0.2}Pt$ alloy. Red circles (blue squares) denote the $\sigma_\parallel$ ($\sigma_\perp$) component of the AHC as a function of the angle θ of the magnetization **M** with [001] axis upon rotating it into the [110] direction. (b) Antiordinary Hall effect in CoPt. Red circles (blue squares) denote the $\sigma_\parallel$ ($\sigma_\perp$) component of AHC as a function of the angle θ of the magnetization **M** with [001] axis upon rotating it into the [110] direction. (c)–(e) depict the relative orientation of the Hall current **J**, AHC $\boldsymbol{\sigma}$, and magnetization **M** in the situation of the antiordinary AHE. In (c)–(e), the magnetization is confined to the $(\bar{1}10)$ plane.

total σ is roughly 170 S/cm [Fig. 5(d)]. With further increasing θ, the magnitude of the AHC is increasing even further, while the AHC vector starts its way toward the [110] direction. The increase of $|\sigma|$ is mainly due to the $\sigma_\perp$ component in this regime, while at the same time $|\sigma_\parallel|$ is becoming smaller, and eventually changes its sign. Finally, at $\theta = 90^\circ$, the AHC vector is aligned together with **M** along the x axis, and its magnitude is 110 S/cm.

Remarkably, $\sigma_\parallel$ turns to zero at $\theta_0 = 70^\circ$, which manifests the occurrence of the *antiordinary* Hall effect in the crystal of CoPt [see Fig. 5(e)]. At this "magic" angle, the magnitude of the anomalous Hall current **J** is almost twice larger than it is for $\mathbf{M}\|z$; however, due to the nonvanishing $\sigma_\perp$ component of the AHC vector, **J** is aligned *along* the direction of the magnetization. By analyzing Figs. 5(b)–5(e), we observe that the rotational sense of the anomalous Hall current is opposite to that observed in the ordinary Hall effect (OHE) of free electron gas. For OHE, Lorentz forces $\sim[\mathbf{H} \times \mathbf{v}]$ are acting on electrons with velocity **v** in the presence of magnetic field **H**. The resulted ordinary Hall current of free electrons is always perpendicular to **H** irrespective of its direction, opposite to the situation of the antiordinary anomalous Hall effect, observed in CoPt. Here, turning the magnetization clockwise in the $(\bar{1}10)$ plane results in an anticlockwise rotation of **J**, with its value staying rather large all the time. The antiordinary *spin* Hall effect has been also recently predicted to occur in transition metals.[16]

In the region of $3d$Pt alloys in the vicinity of $L1_0$ CoPt, the anisotropy of the AHE manifests itself in crucial ways, suggesting new functionalities of the AHE-based devices. In this region, large changes in the magnitude of the anomalous Hall current as well as relative orientation of the Hall current with respect to the magnetization can be easily achieved by simple reorientation of the sample's magnetization. While the former could be used in order to, e.g., tune the relative magnitudes of the extrinsic and intrinsic anomalous Hall signal,[6,29] among the most straightforward applications of the latter could be a realization of the planar Hall effect (PHE),[38] which is related to the Hall effect in ferromagnetic materials observed in a two-dimensional geometry with electric field, with magnetization and the Hall current sharing the same sample plane. So far, it is believed that, in most of the cases, the PHE originates from anisotropic magnetoresistance in metallic ferromagnets, although the PHE mechanism stemming from the anomalous Hall effect due to noncollinearity of the magnetization in semiconductor-based materials has been also suggested.[39] Within the scope of the antiordinary Hall effect, described in this paper, it would be possible to observe the PHE coming solely from the anisotropic nature of the collinear ferromagnetic materials.

We would like to underline that, despite the crudeness of the VCA approximation for the description of the electronic structure of complex alloys, the results of our work still hold, although the exact width of the region where the colossal anisotropy and antiordinary nature of the intrinsic anomalous Hall effect can be observed might be different when more appropriate approximations, such as coherent potential approximation (CPA),[6] are used to treat the substitutional alloys $Fe_xCo_{1-x}Pt$ and $Co_xNi_{1-x}Pt$. The main reason behind this is that, for pure ferromagnets FePt, CoPt, and NiPt, our results are exact in the sense that no approximations of disorder need to be made and the AHE consists only of the intrinsic contribution, while the precise value of the intrinsic AHC will still depend on the chosen parameters and formulations of the DFT calculations such as exchange-correlation functionals, treatment of SOC, validity of the single-particle picture, particular choice of the basis set, etc. The values of the intrinsic AHC at the ends of the considered family of alloys, namely, FePt and NiPt, are large in their magnitude but differ in their sign. This means that, upon varying the concentration x in $Fe_xCo_{1-x}Pt$ and $Co_xNi_{1-x}Pt$ alloys, the region where the AHC changes sign must exist, irrespective of the approximations made. At the end, it is the change of sign of the AHC for the CoPt alloy that leads to the occurrence of the colossal anisotropy and antiordinary anomalous Hall effect in its vicinity according to our calculations.

At the end of this section, we will try to relate the above-mentioned change of sign in the values of the AHC when going from FePt to NiPt to the changes in the electronic structure

of these materials. For this purpose, we first decompose the atomic spin-orbit Hamiltonian in the well-known way:[17]

$$\xi \mathbf{L}\cdot\mathbf{S} = \xi \mathrm{L}_{\hat{n}}\mathrm{S}_{\hat{n}} + \xi(\mathrm{L}^{+}_{\hat{n}}\mathrm{S}^{-}_{\hat{n}} + \mathrm{L}^{-}_{\hat{n}}\mathrm{S}^{+}_{\hat{n}})/2, \tag{8}$$

where ξ is the spin-orbit coupling strength, $\hat{n}$ is the spin magnetization direction (which is taken as the spin-quantization axis), $\mathbf{L}$ and $\mathbf{S}$ are the total orbital and spin angular momentum operators, $\mathrm{L}_{\hat{n}} = \mathbf{L}\cdot\hat{n}$, and $\mathrm{L}^{+}_{\hat{n}}$ and $\mathrm{L}^{-}_{\hat{n}}$ are the corresponding raising and lowering operators (analogously for spin). We shall refer to the first and second terms in Eq. (8) as the spin-conserving and spin-flip parts of the SOC. This terminology refers to the effect of acting with each of them on an eigenstate of $S_{\hat{n}}$. Accordingly, we define $\sigma^{\uparrow\uparrow}$ and $\sigma^{\uparrow\downarrow}$ as the AHC calculated from Eq. (1) after selectively removing the second or the first term on the right-hand side of Eq. (8) from Eq. (2). This is not an exact decomposition, but inspection of Table I shows that it is approximately valid for both magnetization directions in FePt and CoPt, and NiPt with $\mathbf{M}$ along x, i.e., $\sigma^{\mathrm{tot}} \approx \sigma^{\uparrow\uparrow} + \sigma^{\uparrow\downarrow}$ in these cases, while even for NiPt with $\mathbf{M}\|z$, a large discrepancy between the σ^{tot} of -1165 S/cm and the sum $\sigma^{\uparrow\uparrow} + \sigma^{\uparrow\downarrow} \approx -2000$ S/cm does not change the general line of argument that we present below.

By analyzing Table I, we observe that the spin-flip conductivity in $3d$Pt alloys provides a significant contribution to the total AHC, which is particularly striking in case of CoPt where $\sigma^{\uparrow\downarrow}$ is even somewhat larger than the spin-conserving part for both magnetization directions. While in NiPt the AHC anisotropy $\Delta\sigma^{\mathrm{tot}}$ is mainly given by the anisotropy of its spin-conserving part $\Delta\sigma^{\uparrow\uparrow}$, in FePt and CoPt, the anisotropy of the AHC is driven entirely by the anisotropy of $\sigma^{\uparrow\downarrow}$, $\Delta\sigma^{\uparrow\downarrow}$, which exceeds as much as 90% of $\Delta\sigma^{\mathrm{tot}}$ in FePt. Such a pronounced role of the spin-flip SOC for the anomalous Hall conductivity and its anisotropy in ferromagnets containing heavy elements, such as Pt, was demonstrated and explained by Zhang and co-workers by employing the perturbation-theory arguments.[17] In the case of the alloys considered here, from Table I it is, however, clear that despite a large spin-flip contribution, the overall trend of the total AHC between FePt and NiPt can be qualitatively described by considering the spin-conserving AHC only, and we dedicate the rest of the paper to the analysis of $\sigma^{\uparrow\uparrow}$ in FePt, CoPt, and NiPt compounds.

First, the advantage of considering exclusively the spin-conserving SOC is that spin remains a good quantum number, and the conductivity can be unambiguously decomposed into spin-up and spin-down parts: $\sigma^{\uparrow\uparrow} = \sigma^{\uparrow} + \sigma^{\downarrow}$. In particular, this means if we assume that, in the system considered, the spin-orbit is given only by the spin-conserving part, the corresponding spin Hall conductivity σ_{SH} can be obtained as the difference between the spin-resolved conductivities: $\sigma_{\mathrm{SH}} = \sigma^{\uparrow} - \sigma^{\downarrow}$,[3] which implies that, in a nonmagnetic material such as, e.g., Pt, $\sigma^{\uparrow} = -\sigma^{\downarrow}$, while $\sigma_{\mathrm{SH}} = -2\sigma^{\downarrow}$. Second, among the $\sigma^{\uparrow\uparrow}$ and $\sigma^{\uparrow\downarrow}$ conductivities, the latter is much more sensitive to the details of the Fermi surface, while the electronic transitions contributing to the spin-conserving AHC according to Eq. (1) are distributed much broader in energy around E_F,[17] which makes the analysis of the latter easier.

TABLE II. Spin-resolved contributions to the spin-conserving AHC in $3d$Pt alloys. SOC $3d$ (Pt, $3d$ + Pt) stands for the values obtained with SOC on only $3d$ (Pt, both $3d$ and Pt) site(s) included in the calculations. ↑ (↓) denotes the contribution from the majority (minority) spin channel. All values are in S/cm.

		SOC $3d$ + Pt		SOC $3d$		SOC Pt	
		↑	↓	↑	↓	↑	↓
FePt	[001]	612	−35	12	−1	579	−49
	[110]	719	−134	35	225	666	−282
CoPt	[001]	603	−98	14	624	588	−802
	[110]	728	−241	48	400	661	−487
NiPt	[001]	1048	−2562	87	−1607	1032	−2352
	[110]	1589	−1879	215	−1461	1501	−1581

In order to get additional insight into the structure of $\sigma^{\uparrow\uparrow}$, we use the atomic decomposition of the AHC for each spin channel, considered by Zhang *et al.*,[17] based on the following atomic decomposition of the spin-orbit part of the Hamiltonian:

$$H_{\mathrm{SO}} = \xi_{3d}\mathbf{L}^{3d}\cdot\mathbf{S} + \xi_{\mathrm{Pt}}\mathbf{L}^{\mathrm{Pt}}\cdot\mathbf{S}, \tag{9}$$

where $\mathbf{L}^{3d(\mathrm{Pt})}$ is the orbital angular momentum operator associated with $3d$ (Pt) atoms, and $\xi_{3d(\mathrm{Pt})}$ is the spin-orbit coupling strength averaged over the valence d orbitals inside $3d$ (Pt) atom, with the values of 0.54 eV for Pt and 0.05–0.07 eV for $3d$ transition-metal atoms. By selectively turning off the spin-orbit coupling inside $3d$ transition-metal atoms ($\xi_{3d} = 0$) or Pt atoms ($\xi_{\mathrm{Pt}} = 0$), we obtain the values of $\sigma^{\uparrow(\downarrow)}_{\mathrm{Pt}}$ and $\sigma^{\uparrow(\downarrow)}_{3d}$, respectively.

The results of our calculations for the spin and atomically decomposed $\sigma^{\uparrow\uparrow}$ in FePt, CoPt, and NiPt alloys are presented in Table II. Let us take a look at the first two columns of the table, where the values of the total $\sigma^{\uparrow}$ and $\sigma^{\downarrow}$ are listed. First, we observe that positive $\sigma^{\uparrow}$ and negative $\sigma^{\downarrow}$ are opposite in their sign for all alloys. Second, upon going from FePt to NiPt, the spin-up AHC increases but retains its order of magnitude, being about 650 S/cm for FePt and 1300 S/cm for NiPt. On the other hand, a very small spin-down AHC of ≈ -100 S/cm for FePt increases by an order of magnitude and reaches as much as -2500 S/cm in NiPt. Correspondingly, in FePt, the positive sign of $\sigma^{\uparrow\uparrow}$ is due to the AHC in the spin-up channel, while in NiPt, the negative $\sigma^{\uparrow\uparrow}$ is driven by large and negative spin-down AHC.

Consider now the case of FePt. The atomic decomposition of the AHC, presented in Table II, clearly reveals that the large spin-up AHC in this alloy originates from the spin-up contribution of Pt atoms, while the Fe contribution to $\sigma^{\uparrow}$ is very small. In the spin-down channel, Pt and Fe AHCs, both with the magnitude of about 200 S/cm, are opposite in sign and suppress each other. In CoPt, the spin-up Pt and Fe AHCs remain basically the same compared to FePt, while the corresponding spin-down conductivities significantly increase in their magnitude. This can be related to the increase in both Co and Pt density of states of d electrons around the Fermi energy for minority spin, which can be clearly seen in Fig. 6, as compared to respective DOS of FePt alloy. Such an enhancement of the DOS around E_F results in more occupied and unoccupied d states and corresponding transitions across

the Fermi energy, which contribute to the AHC according to Eq. (1), similar to the situation we came across when analyzing the tight-binding-model results previously. While in the latter case the variations of the Fermi energy in the region of increased DOS resulted in large changes of the AHE, in the case of a complex ferromagnet with many bands at E_F in which the AHE is not driven by a single-band degeneracy, it seems reasonable to assume that the increased number of available transitions will lead to a larger magnitude of the AHC. The increased Co and Pt spin-down AHCs are still opposite in sign, however, which still suppresses the total $\sigma^{\downarrow}$, although its value is also somewhat enhanced compared to FePt, which leads to the decrease in overall $\sigma = \sigma^{\uparrow} + \sigma^{\downarrow}$ in CoPt (cf. Table I).

The reason behind increased d DOS of Pt atoms at the Fermi level in CoPt lies in moving of the spin-down Co d subband to lower energies with decreasing exchange splitting. This leads to a stronger hybridization between the Co and Pt d states, which are situated mainly below E_F, and increased Pt DOS (Fig. 6). This is even more pronounced in the case of NiPt, where the spin-down Ni subband lies predominantly below the Fermi energy and the hybridization with the Pt d states is even stronger (Fig. 6). Correspondingly, as a result of even more enhanced spin-down d DOS of Ni and Pt atoms around E_F in NiPt alloy, the values of $\sigma^{\downarrow}_{\mathrm{Ni}}$ and $\sigma^{\downarrow}_{\mathrm{Pt}}$ become very large, reaching as much as -1600 S/cm for Ni and -2300 S/cm for Pt. On the other hand, the increase in Ni and Pt AHC in the majority channel is quite moderate due to slightly enhanced DOS, and the total AHC in NiPt becomes large and negative.

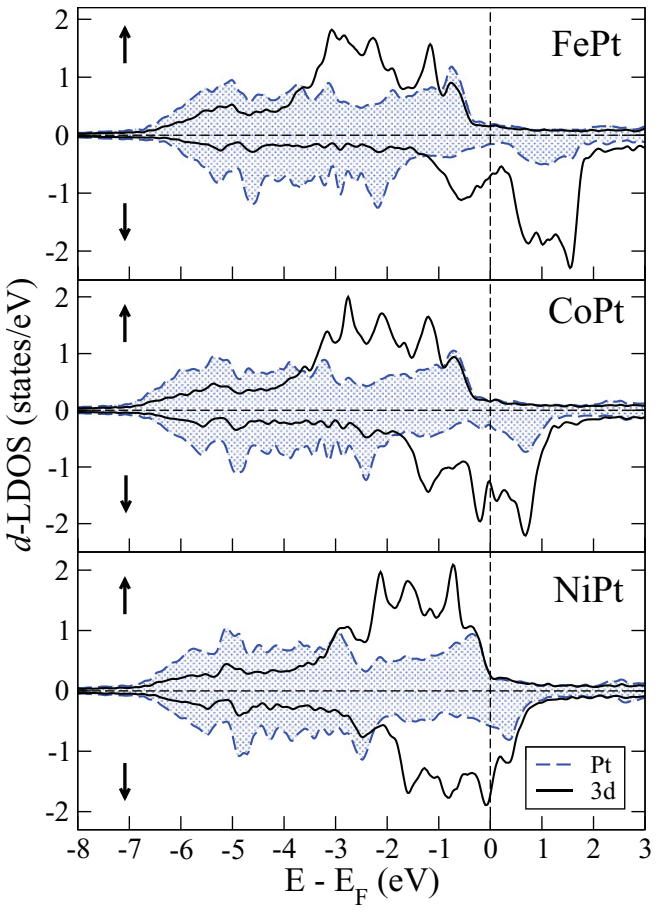

FIG. 6. (Color online) Atomically resolved density of d states in FePt, CoPt, and NiPt alloys. Up and down arrows stand for spin up and spin down.

The change of sign of the 3d spin-down subband AHC between Fe, Co, and Ni in 3dPt alloys can probably be related to different orbital character of the d states at the Fermi energy and corresponding matrix elements of the SOC in these transition metals, which could in turn explain the AHC sign change in elemental Fe, Co and Ni, observed experimentally, and reproduced from the first principles.[9,10,13,14] Such a change of sign as a function of the Fermi level position within the spin subband has been also demonstrated from first-principles calculations of the spin Hall conductivity in Pt,[40] as well as from tight-binding calculations of the spin Hall conductivity in 4d and 5d transition metals.[41] Assuming that, in the latter cases, the spin-flip contribution to the spin Hall effect is negligible,[41] this results in corresponding sign changes of the $\sigma^{\downarrow}$ Hall conductivity, discussed previously.

From Table II, we can see that the AHC originating from the Pt atoms is generally larger in magnitude than that from 3d transition metal. This can be explained by noticing that the large spin-orbit constant inside Pt atoms ξ_{Pt} is by an order of magnitude larger than ξ_{3d}. Moreover, a consistently positive and negative sign of large $\sigma^{\uparrow}_{\mathrm{Pt}}$ and $\sigma^{\downarrow}_{\mathrm{Pt}}$ throughout the 3dPt family can be related to a small spin polarization of the Pt atoms, i.e., under the condition that this spin polarization is at all absent, $\sigma^{\uparrow}_{\mathrm{Pt}}$ should be equal to $-\sigma^{\downarrow}_{\mathrm{Pt}}$, while the difference of the two would provide a value of the intrinsic spin Hall conductivity in Pt of about 2000 S/cm. As we can see from Table II, these arguments indeed explain the sign and magnitude of the Pt-originated AHC. Finally, we would like to remark that, although the atomic decomposition for the spin-resolved conductivities is overall rather reasonable in that $\sigma^{\uparrow} \approx \sigma^{\uparrow}_{\mathrm{Pt}} + \sigma^{\uparrow}_{3d}$ and $\sigma^{\downarrow} \approx \sigma^{\downarrow}_{\mathrm{Pt}} + \sigma^{\downarrow}_{3d}$ (see Table II), such a decomposition works much better for the majority channel. We attribute this observation to a much stronger hybridization of the 3d and Pt d states for the minority spin around the Fermi level, which enhances the contributions to the AHC for which the presence of SOC on both Pt and 3d transition-metal atoms is important. Such contributions are omitted in the atomic decomposition used above.

VI. CONCLUSIONS

In conclusion, we investigated from the first principles the intrinsic anomalous Hall effect in 3dPt alloys. From our calculations, it follows that the AHC in this type of compounds is strongly anisotropic. We demonstrate the generality of such anisotropy in uniaxial ferromagnets by considering a simple three-band tight-binding model. In combination with the sign change of the conductivity upon going from FePt to NiPt, the pronounced AHC anisotropy leads to the occurrence of the colossal anisotropic AHE and antiordinary AHE in the vicinity of the CoPt alloy. While in the case of colossal anisotropic AHE the anomalous Hall current completely vanishes for one of the magnetization directions in the crystal, within the scope of the antiordinary AHE, the rotational sense of the Hall current is opposite to that of the magnetization, and a

complete collinearity of the two can be achieved for a certain magic angle of the magnetization in the crystal. We relate the general trend of the AHC in these alloys to the changes in their electronic structure in the vicinity of the Fermi level, and discuss possible applications of the anisotropic AHE in these compounds.

ACKNOWLEDGMENTS

We acknowledge discussions with I. Souza and F. Freimuth. This work was supported by the HGF-YIG Program VH-NG-513. Computational resources were provided by Jülich Supercomputing Centre.

*h.zhang@fz-juelich.de

[1] E. Hall, Philos. Mag. **12**, 157 (1881).
[2] N. Nagaosa, J. Sinova, S. Onoda, A. H. MacDonald, and N. P. Ong, Rev. Mod. Phys. **82**, 1539 (2010).
[3] J. E. Hirsch, Phys. Rev. Lett. **83**, 1834 (1999).
[4] R. Karplus and J. M. Luttinger, Phys. Rev. **95**, 1154 (1954).
[5] M. Gradhand, D. V. Fedorov, P. Zahn, and I. Mertig, Phys. Rev. Lett. **104**, 186403 (2010).
[6] S. Lowitzer, D. Ködderitzsch, and H. Ebert, Phys. Rev. Lett. **105**, 266604 (2010).
[7] Z. Fang, N. Nagaosa, K. S. Tahakashi, A. Asamitsu, R. Mathieu, T. Ogasawara, H. Yamada, M. Kawasaki, Y. Tokura, and K. Terakura, Science **302**, 92 (2003).
[8] R. Mathieu, A. Asamitsu, K. Takahashi, H. Yamada, M. Kawasaki, Z. Fang, N. Nagaosa, and Y. Tokura, Phys. Rev. Lett. **93**, 016602 (2004).
[9] Y. Yao, L. Kleinman, A. H. MacDonald, J. Sinova, T. Jungwirth, D. S. Wang, E. Wang, and Q. Niu, Phys. Rev. Lett. **92**, 037204 (2004).
[10] X. Wang, J. R. Yates, I. Souza, and D. Vanderbilt, Phys. Rev. B **74**, 195118 (2006).
[11] C. Zeng, Y. Yao, Q. Niu, and H. H. Weitering, Phys. Rev. Lett. **96**, 037204 (2006).
[12] Y. Yao, Y. Liang, D. Xiao, Q. Niu, S. Q. Shen, X. Dai, and Z. Fang, Phys. Rev. B **75**, 020401(R) (2007).
[13] X. Wang, D. Vanderbilt, J. R. Yates, and I. Souza, Phys. Rev. B **76**, 195109 (2007).
[14] E. Roman, Y. Mokrousov, and I. Souza, Phys. Rev. Lett. **103**, 097203 (2009).
[15] I. Yang, S. Y. Savrasov, and G. Kotliar, Phys. Rev. Lett. **87**, 216405 (2001).
[16] F. Freimuth, S. Blügel, and Y. Mokrousov, Phys. Rev. Lett. **105**, 246602 (2010).
[17] H. Zhang, F. Freimuth, S. Blügel, Y. Mokrousov, and I. Souza, Phys. Rev. Lett. **106**, 117202 (2011).
[18] A. A. Hirsch and Y. Weissman, Phys. Lett. A **44**, 239 (1973).
[19] N. V. Volkenshtein, G. V. Fedorov, and V. P. Shirokovskii, Sov. Phys. JETP **11**, 48 (1960).
[20] T. Hiraoka, J. Sci. Hiroshima Univ., Ser. A-2 **32**, 153 (1968).
[21] R. S. Lee and S. Legvold, Phys. Rev. **162**, 431 (1967).
[22] K. Ohgushi, S. Miyasaka, and Y. Tokura, J. Phys. Soc. Jpn. **75**, 013710 (2006).
[23] B. C. Sales, R. Jin, and D. Mandrus, Phys. Rev. B **77**, 024409 (2008).
[24] J. Stankiewicz and K. P. Skokov, Phys. Rev. B **78**, 214435 (2008).
[25] J. Stankiewicz, D. Karpenkov, and K. P. Skokov, Phys. Rev. B **83**, 014419 (2011).
[26] J. Kötzler and W. Gil, Phys. Rev. B **72**, 060412(R) (2005).
[27] A. Cebollada, D. Weller, J. Sticht, G. R. Harp, R. F. C. Farrow, R. F. Marks, R. Savoy, and J. C. Scott, Phys. Rev. B **50**, 3419 (1994).
[28] T. Seki, Y. Hasegawa, S. Mitani, S. Takahashi, H. Imamura, S. Maekawa, J. Nitta, and K. Takanashi, Nat. Mater. **7**, 125 (2008).
[29] K. M. Seemann, Y. Mokrousov, A. Aziz, J. Miguel, F. Kronast, W. Kuch, M. G. Blamire, A. T. Hindmarch, B. J. Hickey, I. Souza, and C. H. Marrows, Phys. Rev. Lett. **104**, 076402 (2010).
[30] [http://www.flapw.de]
[31] J. Perdew, K. Burke, and M. Erzenhof, Phys. Rev. Lett. **77**, 3685 (1996).
[32] P. Ravindran, A. Kjekshus, H. Fjellvåg, P. James, L. Nordström, B. Johansson, and O. Eriksson, Phys. Rev. B **63**, 144409 (2001).
[33] I. Souza, N. Marzari, and D. Vanderbilt, Phys. Rev. B **65**, 035109 (2001).
[34] F. Freimuth, Y. Mokrousov, D. Wortmann, S. Heinze, and S. Blügel, Phys. Rev. B **78**, 035120 (2008).
[35] A. Mostofi, J. R. Yates, Y.-S. Lee, I. Souza, D. Vanderbilt, and N. Marzari, Comput. Phys. Commun. **178**, 685 (2008).
[36] Hongbin Zhang, Ph.D. thesis, Technische Universität Dresden, 2009.
[37] A. Smogunov, A. Dal Corso, and E. Tosatti, Nat. Nanotechnol. **3**, 22 (2008).
[38] K. L. Yau and J. T. H. Chang, J. Phys. F: Met. Phys. **1**, 38 (1971).
[39] M. Bowen, K.-J. Friedland, J. Herfort, H.-P. Schönherr, and K. H. Ploog, Phys. Rev. B **71**, 172401 (2005).
[40] G. Y. Guo, S. Murakami, T.-W. Chen, and N. Nagaosa, Phys. Rev. Lett. **100**, 096401 (2008).
[41] T. Tanaka, H. Kontani, M. Naito, T. Naito, D. S. Hirashima, K. Yamada, and J. Inoue, Phys. Rev. B **77**, 165117 (2008).